Vol. 20, No. 1 (2021) 355-366
Revista Mexicana de Ingeniería Química

Effect of antiscalants and operating variables on the performance of desalination by direct contact membrane distillation (DCMD)

Efecto de antiincrustantes y variables de operación en la eficiencia de desalinización por destilación por membranas por contacto directo (DMCD)

A.L. Peñaranda-López, B. Torrestiana-Sánchez*

[1] *Tecnológico Nacional de México/IT-Veracruz, Unidad de Investigación y Desarrollo en Alimentos. Av. M.A. de Quevedo No. 2779, C.P. 91897, Veracruz, Ver., México.*

Received: March 17, 2020; Accepted: October 19, 2020

Abstract

The effect of hydrodynamic conditions (feed and permeate flow rates) and of six different antiscalants was studied on the desalination of seawater from the Gulf of Mexico by direct contact membrane distillation (DCMD). The effect of feed temperature during the DCMD process was also evaluated on the performance of two microfiltration membranes (0.5 μm) having a different thickness (300 and 250 μm). Results showed more than 100% increments on water vapor flux by raising feed temperature from 50 to 70 oC and feed flow rates up to 7 L min^{-1}. No significant effect on process performance was observed by raising permeate flow rates in the range tested. However, process performance increased by up to 49.2% during the desalination of real seawater by adding the KMRO S-516 antiscalant, designed to disperse iron, silica, and calcium carbonate salts. Antiscalant dosage did not induce important water vapor flux decay or increase the conductivity of the distillate during DCMD. Scanning electron microscopy (SEM) from the membrane surface after DCMD desalination of seawater, treated with the KMRO S-516 antiscalant, evidenced the absence of scaling. Results from this work confirmed that the type and concentration of antiscalants are critical during seawater desalination by DCMD.

Keywords: Antiscalant, seawater, desalination, operation conditions, direct contact membrane distillation.

Resumen

Se evaluó el efecto de las condiciones hidrodinámicas y de seis antiincrustantes durante la desalinización de agua del Golfo de México mediante destilación por membranas por contacto directo (DMCD). El efecto de la temperatura de alimentación también se evaluó durante el proceso con dos membranas de microfiltración (0.5 μm) de diferente espesor (300 y 250 μm). Se obtuvieron incrementos de más del 100% en el flux cuando se aumentó la temperatura de alimentación de 50 a 70 °C y del caudal de alimentación a 7 L·min^{-1}. No se observó un efecto significativo en el flux con el incremento del caudal de permeado. Sin embargo, el flux incrementó un 49.2% cuando se agregó el antiincrustante KMRO S-516, diseñado para la dispersión de hierro, silica y sales de carbonato de calcio. La adición de antiincrustantes durante la DMCD no afectó el flux de permeado ni la conductividad del destilado. El análisis por microscopia electrónica de barrido (SEM) de la superficie de la membrana después de la desalinización del agua de mar empleando el antiincrustante KMRO S-516 confirmó la ausencia de incrustaciones. Los resultados indicaron que el tipo de antiincrustante y su concentración son críticos para el proceso.

Palabras clave: Antiincrustante, agua de mar, desalinización, condiciones de operación, destilación por membranas por contacto directo.

1 Introduction

Water is the most important natural resource on Earth, and in Mexico, coastal regions have large water volumes, but with high concentrations of salt, thus they cannot be considered as sources of drinking water. With the increase of the population and over exploitation of water resources, the reserves of this vital liquid are affected. These reserves are decreasing at a rate of 6 km^3/year, where more than 70% is used in the agricultural sectors, 5% in the industry sectors and 14% in the public sector (García-Chávez *et al*., 2020).

* *Corresponding author. E-mail*: beatriz.ts@veracruz.tecnm.mx
https://doi.org/10.24275/rmiq/Proc1457
ISSN:1665-2738, *issn-e*: 2395-8472

Desalination of seawater and brackish groundwater have been used to obtain fresh water in some arid countries, where water scarcity is severe. Currently, reverse osmosis (RO) is the worldwide preferred desalination process, but its main drawbacks are insufficient boron removal and its high energy consumption due to the high operating pressures required (Lee *et al*. 2011; Hou *et al*. 2013). Membrane distillation (MD) is a thermally driven process, that can be used in a wide variety of applications such as desalination and wastewater treatment. In MD at least one side of a microporous hydrophobic membrane is in contact with an aqueous solution. In contrast to other membrane technologies, the driving force in this process is the partial pressure difference induced by a temperature gradient between two sides of the membrane. In this process, only vapor molecules can pass through the membrane due to the hydrophobicity of the membrane (Kebria and Rahimpour 2020). MD is not restricted by the feed salinity (as in the RO) and its low thermal requirements (compared with thermal distillation) offer an alternative where conventional separation processes are challenged (Naidu *et al*. 2015). Four main configurations differ from each other by their condensation procedure: Air gap membrane distillation (AGMD), sweeping gas membrane distillation (SGMD), vacuum membrane distillation (VMD) and direct contact membrane distillation (DCMD) (Kebria and Rahimpour 2020). For field/commercial applications the focus has been on AGMD and VMD configurations (Adham *et al*., 2013). The benefit of these designs is reduced (for AGMD) or even negligible (for VMD) heat loss by conduction (Alkudhiri *et al*., 2012; Naidu *et al*., 2015). However, DCMD has been widely investigated in the study of desalination processes, due to its simplest configuration (Alkhudhiri *et al*., 2012; Adham *et al*., 2013). It has been reported that operating conditions affect markedly the heat and mass transfer during DCMD. Feed temperature has a strong influence on the process performance, having even an exponential effect on the water flux (Song *et al*., 2007; Al-Obaidani *et al*., 2008; Alkudhiri *et al*., 2012). This is due to the increase in water vapor pressure (the driving force of the process), which according to the Antoine equation, increases exponentially with temperature (Alkudhiri *et al*., 2012, Ali *et al*., 2013). It has been reported that the solution flow rate may also affect process efficiency, because the boundary layer resistance to heat and mass transfer decreases as the feed flow rate is increased (Ali *et al*. 2013; Zhu *et al*. 2015). Membrane thickness is another important factor in DCMD because mass transfer resistance increases with the thickness (Shirazi *et al*. 2014), but a large amount of heat can be transferred by conduction when a thin membrane is used, and this affects process performance (Gryta 2012a).

Nevertheless, operation conditions are not the only factors that affect the efficiency of the process. The main drawback of the MD process is scaling on the membrane surface when the concentrations of sparingly soluble dissolved salts (e.g., $CaCO_3$, SiO_2, $BaSO_4$, etc.) near the membrane surface rise above their solubility limits. As a result, deposits of salt on the pore mouth allow moisture condensing and that leads to pore wetting, decreasing flux, and salt rejection (Li and Sirkar 2005). Among inorganic contaminants, calcium carbonate ($CaCO_3$) and calcium sulfate ($CaSO_4$) are widely found in desalination processes (Peng *et al*. 2015). A common method to control scaling in conventional desalination processes is adding small doses of a low-cost anti-scaling agent in the feed side (Warsinger *et al*. 2015). This is a cost-effective approach since in many cases scaling can be avoided with less than 10 mg L^{-1} of the antiscalant (He *et al*., 2009). However, most studies of desalination by direct contact membrane distillation have focused on the use of antiscalants to prevent fouling by using synthetic brines (He *et al*. 2009; Zhang *et al*., 2015, Gryta *et al*., 2012b). For example, He *et al*. (2009) observed during the DCMD of supersaturated synthetic brine that antiscalants GHR (a nitrogen-containing organo-phosphorus solution) and K752 (a polyacrylic acid solution) prolonged substantially the induction period of calcium sulfate and calcium carbonate, even at dosage levels as low as 0.6 mg L^{-1}. Similarly, Zhang *et al*. (2015) used an organic phosphonate solution (Flocon 190) on the DCMD of a concentrated synthetic seawater brine. They reported that the addition of Flocon 190 helped to delay salt precipitation and flux reduction primarily caused by precipitation of $CaCO_3$ and $CaSO_4$. However, a steeper flux decline was observed by Gryta (2012b) when a polyphosphate-based antiscalant, designed for reverse osmosis, was added during DCMD of tap water enriched in HCO_3^- ions. This antiscalant restricted the deposits formed; however, an amorphous low porous layer was deposited onto the membrane surface instead of crystallites and this lowered the permeate flux after 5 h of operation.

Therefore, more effort is needed to fully understand the role of different factors involved in determining the effectiveness of antiscalants in

direct contact membrane distillation. In this work, the combined effect of operating conditions (feed temperature as well as feed and permeate flow rates) and the effect of 6 different commercial antiscalants recommended for reverse osmosis on the performance of direct contact membrane distillation was evaluated during desalination of seawater from the Gulf of Mexico. The process was conducted by using two microfiltration membranes having similar average pore size (0.5 μm) but different thickness (300 and 250 μm).

2 Theory

Membrane distillation is a process characterized by simultaneous mass and heat transfer in the membrane and the bulk liquid phases. Heat transfer (q) takes place in three steps: heat transfer from the bulk feed side to the membrane surface (q_F), the transfer of heat through the membrane (q_m), and the heat transferred from the membrane surface to the bulk of the permeate (q_P). At steady state (Ibrahim and Alsalhy 2013):

$$q_F = q_m = q_P \tag{1}$$

However, due to temperature polarization, the temperatures at the liquid-membrane interface (T_{mF}, T_{mP}) may vary markedly from the measurable bulk temperatures (T_F, T_P). Therefore, Eq (1) can be rewritten as Eq. (2) (Ibrahim and Alsalhy 2013):

$$\begin{aligned} A_o h_F (T_F - T_{mF}) &= A_{r\ ln} h_m (T_{mF} - T_{mP}) + A_{ro} J\lambda \\ &= A_i h_P (T_{mP} - T_P) \end{aligned} \tag{2}$$

where h_F and h_P represent the heat transfer coefficients for the feed and permeate side, respectively. T_F, T_{mF}, T_P, and T_{mP} are the bulk and liquid-membrane interface temperatures at the feed and permeate sides (according to the subscripts), J is the flux, λ is the latent heat of vaporization and A_o and A_i are fibers area considering the outside (r_o) and inside (r_i) ratio of the fiber respectively. $A_{r\ ln}$ is defined as:

$$A_{r\ ln} = (A_o - A_i) / \ln (A_o / A_i) \tag{3}$$

The phenomenon of temperature polarization causes an important loss in the driving force. Hence, the temperature polarization coefficient (τ) is used to describe the thermal efficiency of the process. This is defined as the ratio of the difference of temperatures at the membrane surfaces on feed and permeate sides to the corresponding difference in the bulk (Martínez and Vázquez 1999; Ali *et al*., 2013):

$$\tau = \frac{T_{mF} - T_{mP}}{T_F - T_P} \tag{4}$$

When the value of τ approaches unity, it describes a thermally efficient process.

o estimate the value of τ, the temperatures at the membrane surface in the feed and permeate sides can be obtained by combining the equations describing the heat stream density flowing across the membrane and the boundary layer equations (Ibrahim and Alsalhy 2013):

$$T_{mF} = \frac{h_m (T_P + (h_F / h_P) T_F) + h_F T_F - J\lambda}{h_m + h_F (1 + (h_m / h_P))} \tag{5}$$

and

$$T_{mP} = \frac{h_m (T_F + (h_P / h_F) T_P) + h_P T_P - J\lambda}{h_m + h_P (1 + (h_m / h_F))} \tag{6}$$

here h_m is defined as (Bui *et al*. 2010):

$$h_m = \frac{k_m}{r_i \ln(r_o / r_i)} \tag{7}$$

k_m is the thermal conductivity of the porous membrane that can be calculated as:

$$k_m = \epsilon k_g + (1 - \epsilon) k_s \tag{8}$$

where ϵ is the membrane porosity, k_g and k_s are the thermal conductivities of air and membrane material (polymer), respectively. The feed and permeate film heat transfer coefficients (h_F and h_P) can be calculated by the dimensionless Nusselt number:

$$h_i = \frac{Nu_i k_i}{d_h}; \quad i = F, P \tag{9}$$

where k is the fluid thermal conductivity and d_h is the hydraulic diameter. The heat transfer coefficient for the seawater (outside the fibers) has been estimated with the following correlation of the Nusselt number (Nu_F):

$$Nu_F = 0.36 Re_F^{0.55} Pr_F^{1/3} \tag{10}$$

Equation (10) has been used to estimate the heat transfer coefficient on the shell side of shell and tube heat exchangers (Valdés *et al*., 2009). The Nusselt number on the permeate (Nu_P) (inside the fibers), was calculated using Eq. 11, which has been developed for laminar flow into a tube (Valdés *et al*., 2009):

$$Nu_P = 3.66 + \frac{0.0668\, Re_P\, Pr_P (D/L)}{1 + 0.04\, Re_P\, Pr_P (D/L)^{2/3}} \qquad (11)$$

where Reynolds number, $Re = v_i d_h \rho_i / \mu_i$ and Prandtl number, $Pr = Cp_i \mu_i / k_i$, with $i = F, P$. Further v is the linear velocity, ρ is the liquid density, μ is the dynamic viscosity, Cp is the liquid heat capacity, k is the fluid thermal conductivity, and D and L are the diameter and length of the fibers. For Eq. 10 to be valid, $Re < 2{,}300$. Eqs. (10) and (11) have been used to model heat transfer in the osmotic distillation process with hollow fibers (Peñaranda-López *et al.*, 2016; Valdés *et al.*, 2009).

To obtain the value of τ an iterative solution is required and initial values of T_{mF} and T_{mP} are assumed. Then, using experimental data for J, the values of the h coefficients are calculated from Eqs (8-10) at the average temperatures $(T_F + T_{mF})/2$ and $(T_P + T_{mP})/2$. From Eqs (4) and (5), the temperatures T_{mF} and T_{mP} are obtained when the relative error, between the calculated and the assumed initial values, is equal to 0.1%.

3 Methods

3.1 Feed solutions and antiscalants properties

Water from the Gulf of Mexico (Veracruz, Mexico) was used as a feed solution with a salinity of 36 g L^{-1} (National Centers for Environmental Information). This was previously filtered through a 0.22 μm membrane. The properties of the antiscalants tested and their recommended dosage was provided by the manufacturer (Table 1).

3.2 Turbidity test

The effectiveness of antiscalants to prevent scaling was indirectly evaluated in a turbidity test by using calcium carbonate ($CaCO_3$), one of the most important inorganic pollutants in desalination. A supersaturated solution of $CaCO_3$ was prepared by mixing (for 15 minutes), equimolar (1.6 M) solutions of reagent grade (J.T. Baker) calcium chloride ($CaCl_2$), and sodium carbonate ($NaHCO_3$), dissolved in distilled water. As a result, $CaCO_3$ crystals are formed and the turbidity of the saturated solution is evaluated at 520 nm, using a spectrophotometer (DU 7500, Beckman). To evaluate the effectiveness of previously selected antiscalants, these were dosed and mixed with the supersaturated $CaCl_2$ solution for 10 min, before adding the $NaHCO_3$ solution. The turbidity of these solutions was also determined at 520 nm.

3.3 Experimental setup and process conditions

The experimental set up used in this work is shown in Fig. 1. Two hollow fiber membrane contactors (Markel®) were used. The membranes had 23 polytetrafluoroethylene (PTFE) fibers and 0.054 m2 of the total surface area. The fibers were 250 mm long, 3.5 mm in diameter, 300 μm (M1), and 250 μm (M2) thickness and presented an average pore size of 0.5 μm (Table 2).

Table 1. Main composition and properties of antiscalants tested in direct contact membrane distillation of seawater (Kurimexicana S.A. de C.V.).

Antiscalant	Properties	Recommended dosage (mg L^{-1})
KMRO S-502	Inhibits silica fouling	10
KMRO S-512	Silica antiscalant. Inhibits also fouling of $CaCO_3$ and iron	10
KMRO S-514	Silica antiscalant. Inhibits also fouling of $CaSO_4$, $BaSO_4$ and $SrSO_4$	10
KMRO S-516	Inhibits mainly iron and $CaCO_3$ fouling. Acts also on silica.	10
GLF	Silica antiscalant. Inhibits also scales from $CaCO_3$, $CaSO_4$, $Ca_3(PO_4)_2$, $BaSO_4$, $SrSO_4$, silica and iron/manganese.	5
GSI	Inhibits scales from $CaCO_3$, $CaSO_4$, $Ca_3(PO_4)_2$, $BaSO_4$, $SrSO_4$, silica, iron/Manganese	5

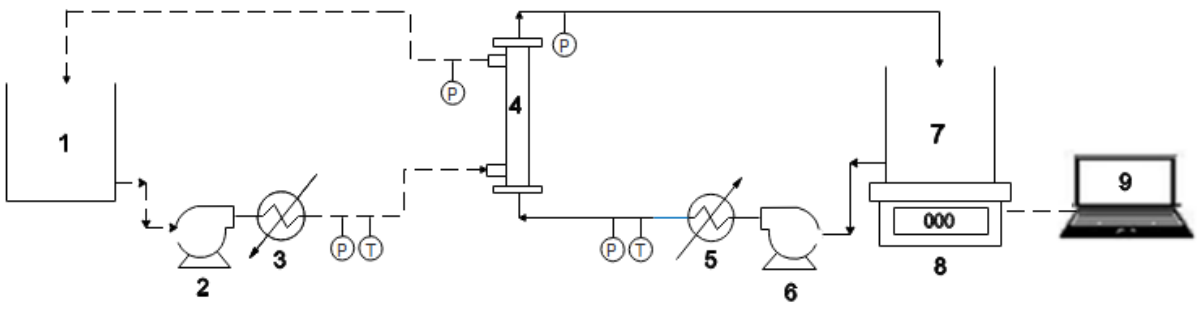

Fig. 1. Experimental set up for direct contact membrane distillation. 1. Seawater tank; 2. Feed pump; 3. Feed heat exchanger; 4. Membrane module; 5. Permeate heat exchanger; 6. Permeate pump; 7. Permeate tank; 8. Scale; 9. Computer.

Table 2. Technical specifications of the hollow fiber polymeric membranes.*

Property	M1	M2
Number of fibers	23	23
Fiber lenght (mm)	250	250
External fiber diameter (mm)	3.5	3.5
Porosity	≥0.65	≥0.65
Pore size (μm)	0.5	0.5
Thickness (μm)	300	250

*Supplied by the manufacturer (Markel®).

Peristaltic pumps equipped with a variable frequency drive were used to recycle permeate and seawater through and outside the fibers, respectively. A calibration curve of frequency (Hertz) versus flow rate was prepared before the experiments. The flow rate was obtained by automatically recording the weight gain of water collected in a reservoir as a function of time by using a precision balance connected to a computer.

The temperature of feed and permeate solutions at the inlet of the membrane module were maintained by using heat exchangers. Pressure on both sides of the membrane was monitored by pressure sensors located at the inputs and outputs of the module. The volume of feed and permeate solutions used were similar (1.5 L). Seawater desalination was carried out under two different feed (Q_F: 0.8 L min^{-1} and 7 L min^{-1}) and permeate flow rates (Q_P: 0.8 L min^{-1} and 1.6 L min^{-1}) as well as feed solution temperatures (T_F: 50 °C and 70 °C). When Q_F = 7 L min^{-1} a pressure of 0.03 kPa cm^{-2} was detected on the feed side, but no pressure above atmospheric pressure was detected by the sensor at the same location at the lower feed rate (Q_F=0.8 L min^{-1}). The temperature of the permeate side was kept constant at 10 °C in all cases. It has been reported that partial pore wetting will decrease salt rejection and water vapor flux during the process (Li and Sirkar 2005). Hence the entrance of saline solution into the membrane pores resulting from pore wetting by salts or the antiscalant may cause an increase in distillate conductivity (He *et al*., 2009). To avoid this, permeate conductivity was measured at the beginning and the end of every experiment utilizing a conductivity meter (Thermo Scientific Orion Star A215). Seawater conductivity was also registered at the beginning and the end of each experiment. Process performance in terms of the vapor permeate flow rate was monitored via the weight gain of the permeate tank by using a precision balance branched to a computer (Fig. 1). Permeate flux (J) was calculated from the collected data by equation 12 (Hou *et al*., 2013):

$$J = \frac{W_2 - W_1}{(t_2 - t_1) * A} \tag{12}$$

where A is the membrane area, W_2 and W_1 are permeate weight at time 2 (t_2) and time 1 (t_1) respectively.

3.4 Membrane cleaning

After every run, membranes were cleaned by using a base-acid protocol. This starts by recycling distilled water at room temperature for 15 minutes. Then, a sodium hydroxide solution (3% w/w) is recycled at 40 °C for 45 minutes followed by rinsing with distilled water until pH=7.0. Finally, a citric acid solution (3% w/w) was recycled at 40 °C for 45 minutes. Rinsing with distilled water was repeated until water pH was 7.0. Water vapor flux was measured, before every experiment and after membrane cleaning, using

deionized water as feed, to verify the efficiency of the cleaning protocol.

3.5 Scanning electron microscopy (SEM)

The PTFE membrane surface was characterized by using scanning electron microscopy (FEI, Quanta FEG 450) at the end of the final experiment since this analysis is destructive, and we did not want to affect the integrity of the hollow fiber module before experimentation. It is important to note that the sample of the membrane sample M2 analyzed by SEM was not submitted to the cleaning protocol after the run conducted under the best experimental conditions (i.e. antiscalant type and dosage). A sample of clean M1 membrane was also analyzed by SEM since all properties, except thickness, of both membranes, were similar. Before the analysis, membrane samples were attached to the grid using carbon copper tape and sputtered with gold by a sputter coater (Quorum Q150R S, Quorum Technologies Ltd.).

4 Results and discussion

4.1 Effect of operation conditions on water vapor flux

The effect of feed and permeate flow rates, as well as feed temperature, was first evaluated with the two membranes tested. Fig. 2 shows the water vapor flux obtained from both 0.5 μm membranes having 300 μm (M1) and 250 μm (M2) thickness under different permeate flow rates (Q_P), seawater flow rates (Q_F) and temperatures (T_F). Results from Fig. 2 points out that even though both membranes have the same pore size, the membrane with a larger thickness (M1) shows a better performance than the thinner one (M2), especially when the process was conducted under the higher feed flow rate (7 L min^{-1}) and temperature (70 °C) tested. This can be the result of the high amount of heat being transferred from the feed to the permeate, which was less efficiently dispersed in the permeate side of the thinner membrane (M2), since both membranes have similar properties (nature, microstructure, pore size, porosity, and geometry) except thickness (Table 2). The efficiency of the membranes is compared in terms of the temperature polarization coefficient (τ) in Table 3. Results show that M1 was more efficient than M2, under all tested conditions. Similar results were reported by Adham *et al.* (2013), who tested 0.2 and 0.45 μm PTFE membranes having a thickness between 120 and 230 μm and found that the thicker membranes had the highest flux. Shirazi *et al.* (2014) also observed that 0.22 μm membranes with 230 μm thickness had superior performance than membranes having a thickness of 175 μm.

Fig 2 also shows more than 100% flux increments in both membranes when the feed temperature is increased from 50 to 70 °C. It can be seen from Fig. 2 that when the M1 membrane operated under a Q_F = 7 L min^{-1} and Q_P=0.8 L min^{-1}, a temperature rise from 50 to 70 °C, led to a flux increase from 2.7 to 6.1 kg m^{-2} h^{-1}. The positive effect of raising the temperature on membrane performance is the result of increments on the partial pressure of water in the liquid-membrane interface, which increases the driving force. Similar results were reported by Al-Obaidani *et al.* (2008) during the DCMD of model seawater solutions having 35 g L^{-1} NaCl. They increased the feed temperature from 25 to 60 °C while keeping the permeate temperature at 15 °C and observed that flux increased exponentially, in the four polypropylene membranes tested, as a consequence of the increase in the driving force.

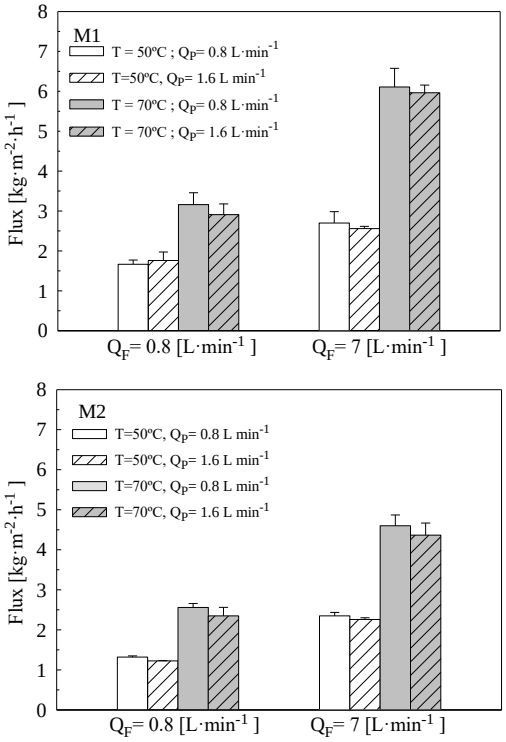

Fig. 2. Effect of feed temperature and feed (Q_F) and permeate (Q_P) flow rates on flux profiles of both M1 and M2 membranes.

Table 3. Temperature polarization coefficients (τ) and the corresponding temperature gradients between the bulk liquid and membrane surfaces. The permeate side temperature was kept constant at 10 °C in all cases.

Q_F (L min^{-1})	Q_P (L min^{-1})	T_F (ºC)	M1		M2		τ(Eq. 4)	
			$T_F - T_{mF}$ (ºC)	$T_{mP} - T_P$ (ºC)	$T_F - T_{mF}$ (ºC)	$T_{mP} - T_P$ (ºC)	M1	M2
0.8	0.8	50	4.71	12.31	4.63	12.5	0.52	0.481
	1.6	50	4.84	12.74	4.74	12.87	0.518	0.482
	0.8	70	7.48	17.32	7.37	17.67	0.504	0.467
	1.6	70	7.63	17.79	7.47	18.08	0.506	0.468
7	0.8	50	1.6	13.64	1.58	13.85	0.558	0.518
	1.6	50	1.61	13.77	1.59	14.04	0.56	0.519
	0.8	70	2.79	20.67	2.65	20.34	0.535	0.505
	1.6	70	2.82	21.03	2.66	20.5	0.537	0.507

Increments in the feed flow rate also had a positive effect on flux. Fig 2 shows that raising the feed flow rate from 0.8 to 7 L min^{-1} increased flux between 46.7 and 122%, leading to a maximum value of 6.1 kg m^{-2} h^{-1}. Similar results were obtained by Zhu *et al*. (2015) who reported that flux almost doubled by increasing feed flow rate from 40 to 120 L h^{-1} and keeping the feed and permeate temperatures in 65 and 17 °C, respectively. Increments in the feed flow rate increased the temperature polarization coefficient (τ) indicating a more efficient process (Table 3), hence the temperature gradient across the membrane and consequently the driving force (vapor pressure difference) are kept higher in the tested range of temperature. A higher feed flow rate also decreases concentration polarization (Appendix A), and this helps increasing the driving force by lowering the salt concentration at the membrane surface. However, results demonstrated that concentration polarization effect was lower than the temperature polarization in the DCMD process. Data from Table 5 show that the concentration polarization (ζ) at the membrane surface was up to 0.51% higher than the bulk concentration and it decreased to 0.13% when increasing the feed flow rate from 0.8 to 7 L min-1 at 70 ºC.

Moreover, increasing permeate flow rates between 0.8 and 1.6 L min^{-1} did not have a significant effect on process performance. This is because the increment in the permeate flow rate was smaller than that to the feed and it was not enough to decrease the temperature polarization at the permeate side caused by the large amount of heat transferred to the permeate, which lowers the temperature gradient across the membrane (Table 3), and consequently the vapor pressure gradient. The conductivities of feed and permeate were registered at the beginning and at the end of experiments to make sure that no diffusion of salt occurred from the feed to the permeate side. In the retentate, seawater conductivity varied from 52.9 to 59 mS cm^{-1}, while the permeate conductivity remained between 5.9 and 6.1 μS cm^{-1}, under all experimental conditions.

4.2 Effect of antiscalants on water flux

The effectiveness of the different antiscalants on the DCMD process performance was compared for the M2 membrane by using 10 mg L^{-1} dosage and the best-operating conditions of Q_P (0.8 L min^{-1}), Q_F (7 L min^{-1}) and T_F (70 °C) previously determined. The M2 membrane was tested to compare the effect of scaling regarding the heat lost by conduction in this membrane.

The results from Fig. 3 suggest that all the antiscalants tested had a positive impact on water vapor flux. From the best to the less effective, antiscalants can be listed in the following order: KMRO S-516> KMRO S-502>Genesys LF> KMRO S-512> Genesys SI>KMRO S-514. The different antiscalants seem to affect even in the early stage of the process, where some salt ($CaCO_3$) precipitation might occur due to the shift of bicarbonate ion to the carbonate and hydroxide ions, when the seawater is heated (Gryta 2012 b):

$$Ca^{2+} + 2HCO_3^- \longrightarrow CaCO_3 + CO_2 + H_2O$$

Therefore, the higher flux values obtained when adding the KMRO S-516 antiscalant is because it inhibits mainly $CaCO_3$ fouling (Table 1). Phosphate-containing antiscalants (i.e KMRO S-516), prevent the scale deposition by sequestering calcium and inhibiting scale precipitation.

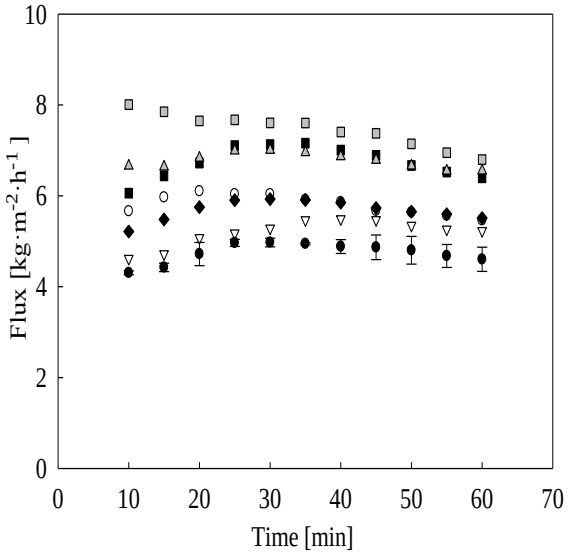

Fig. 3. Effect of antiscalants on water vapor flux of M2 membrane (250 μm thickness) during seawater desalination by DCMD. K 516 (▣) K 502 (△) G LF (▪) K 512 (○) G SI (◆) K 514 (▽), without antiscalant (●).

Usually, the mechanism suggested for the scale inhibition is the adsorption of antiscalant on the crystal surface, blocking the active crystal growth sites. After the adsorption, several modes of action can be considered such as slow down crystal growth rate, delaying germination, and deforming the crystal, giving them a friable structure that weakens its adherence to the surface (Ketrane *et al*., 2009). These results agree with those reported by Gryta 2012b, who kept a solution of 3.1 mmol HCO_3^-/L, with and without a polyphosphate antiscalant at 84 °C and found a decline in the concentration of HCO_3^- ions after 30 minutes.

Differences in the flux profile observed in the presence of the antiscalants tested might be related to their chemical composition and their anti-scaling properties. For example, according to the technical specifications (Table 1), the GLF antiscalant also inhibits fouling by $CaCO_3$, however, the mechanism of preventing fouling may be different to that from KMRO S-516, i.e. interference of the crystal growth and nucleation of salts (Hou *et al*., 2013), and that is why it takes about 30 min to reach its maximal efficiency.

4.3 Turbidity test

The effectiveness of antiscalants (KMRO S-516 and KMRO S-502) to decrease crystal growth and probably salt nucleation was indirectly evaluated in a turbidity test with a supersaturated $CaCO_3$ solution. Results showed that the turbidity of the supersaturated solution was not significantly reduced by adding the antiscalant KMRO S-502 in the concentration range tested (Table 4). However, turbidity drastically decreased when K 516 was added, especially with a 10 mg L^{-1} dosage. This result showed that antiscalant type and the dosage is an important issue in the process and that the antiscalant KMRO S-516 strongly prevents the formation of $CaCO_3$ crystals, which is the main foulant in the desalination process.

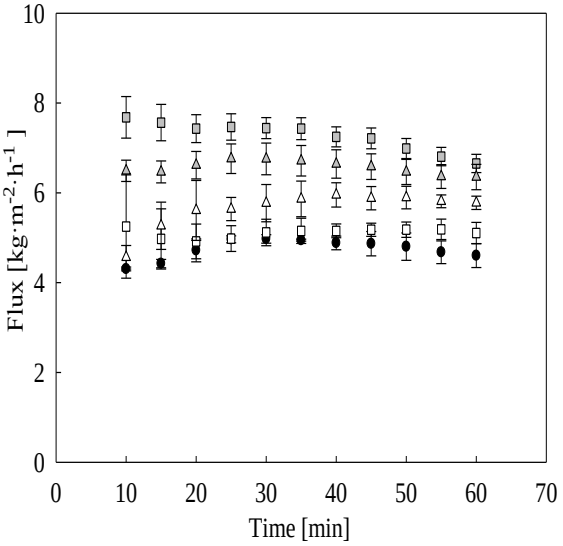

Fig. 4. Effect of antiscalant concentration on performance of M2 membrane (thickness 250 μm) during seawater desalination by DCMD. K 516 at 10 mg L^{-1} (▣) K 502 at 10 mg L^{-1} (△) K 516 at 5 mg L^{-1} (□) K 502 at 5 mg L^{-1} (△), without antiscalant (●).

Table 4. Effect of antiscalants concentration on turbidity of supersaturated $CaCO_3$ solution.

Antiscalant	**Dosage (mg L^{-1})**	**Absorbance** (520 nm)
K 516	5	0.0148
	10	0.0012
K 502	5	0.1274
	10	0.1242
Without antiscalant	–	0.1756

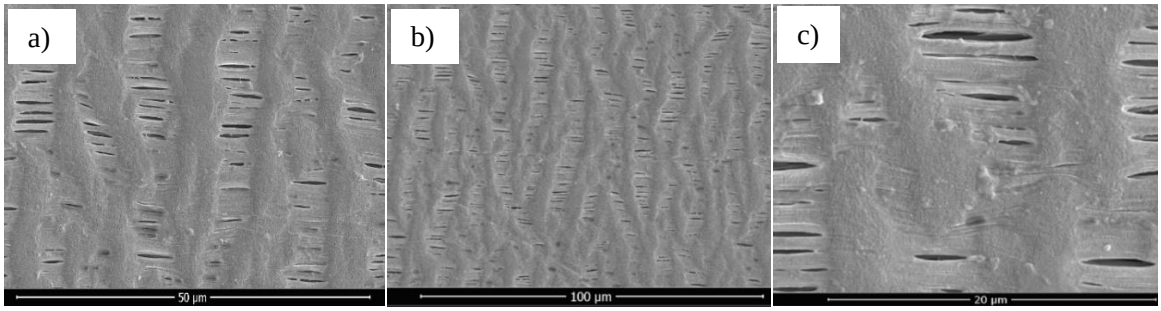

Fig. 5. SEM micrographs from the surface of clean M1 membrane (a) and from the M2 membrane surface after the DCMD desalination process conducted with seawater treated with the KMRO S-516 antiscalant (b, c).

Table 5. Concentration polarization coefficient (ζ) obtained under the tested experimental conditions.

Q_F (L min^{-1})	Q_P (L min^{-1})	T_F (ºC)	ζ M1	ζ M2
0.8	0.8	50	1.003	1.0025
	1.6	50	1.0032	1.0023
	0.8	70	1.0051	1.0043
	1.6	70	1.005	1.0042
7	0.8	50	1.0006	1.0006
	1.6	50	1.0006	1.0006
	0.8	70	1.0013	1.001
	1.6	70	1.0013	1.001

4.4 Effect of antiscalants concentration on water vapor flux

The effect of antiscalant concentration on DCMD process performance was evaluated with both KMRO S-516 and KMRO S-502 anti-scaling agents. Fig. 4 shows the flux profile overtime during desalination of seawater without and with antiscalants at two different concentrations (5 and 10 mg L^{-1}). It can be seen that flux increased with antiscalant addition especially at the highest concentration tested (10 mg L^{-1}). Experimental data show that the flux for the M2 membrane increased by about 36% when 10 mg L^{-1} of KMRO S-502 was added but it increased 49% with KMRO S-516, at the same concentration.

The best performance (7.2 kg m^{-2} h^{-1}) was registered with the KMRO S-516 at 10 mg L^{-1}. This flux was even higher to that obtained with the M1 membrane (6.57 kg m^{-2} h^{-1}) at the same operating conditions but without antiscalant (see Fig. 1).

It can be concluded that scaling, under tested conditions, has a higher influence on the process performance than the reduction of the temperature gradient induced by the small thickness of the membrane. These results agree with experimental data obtained from the turbidity test and confirm that $CaCO_3$ is the main foulant in seawater desalination. Results from Fig. 4 also indicate that the dosage of KMRO S-502 or KMRO S-516 antiscalants did not affect flux stability during the process.

The conductivity of the permeate determined at the end of the experiments was similar with and without antiscalants, i.e. 6.12 μS cm^{-1} and 6.04 μS cm^{-1}, respectively. This suggests that salt diffusion from the feed to the permeate did not occur, and neither happened the partial or complete wetting of the membrane pore due to antiscalant addition.

4.5 Scanning electron microscopy (SEM)

SEM images of membrane M2 (Fig. 5b and 5c) taken after the DCMD desalination process conducted with seawater treated with 10 mg L^{-1} of the KMRO S-516 antiscalant are compared with a micrograph from the clean M1 membrane since both have similar properties (microstructure, pore size, and porosity) except thickness. Results confirmed the absence of salt deposits onto the M2 membrane surface, and therefore the efficiency of this antiscalant to avoid crystal formation of salts under the experimental conditions tested.

Conclusions

- Results from this work point out that the type and concentration of antiscalants play an important role during seawater desalination by direct contact membrane distillation. The performance of this process increased by up to 49.2% during the desalination of seawater from

the Gulf of Mexico by adding a commercial antiscalant designed to disperse mainly calcium carbonate salts.

- No important water vapor flux decay and no increase in the conductivity of the distillate was observed due to the dosage of antiscalants.

- Results also showed increments of more than 100% in terms of water vapor flux by increasing the temperature from 50 to 70 °C, and feed flow rates up to 7 L min^{-1}, while no significant effect on process performance was determined by raising permeate flow rates in the range tested.

Acknowledgements

Authors wish to thank the UNIDA at the Tecnológico Nacional de Mexico/IT-Veracruz for the facilities and technical support given to carry out this work. Alba L. Peñaranda-López also thanks the Consejo Nacional de Ciencia y Tecnología (CONACyT) for the scholarship granted during her graduate studies.

References

Adham, S., Hussain, A., Matar, J.M., Dores, R. and Janson, A. (2013). Application of membrane distillation for desalting brines from thermal desalination plants. *Desalination 314*, 101-108. https://doi.org/10.1016/j.desal.2013.01.003

Ahmad, S., Marson, G., Zeb, W., Rehman, W., Younas, M., Farrukh, S. and Rezakazemi, M. (2020). Mass transfer modelling of hollow fiber membrane contactor for apple juice concentration using osmotic membrane distillation. *Separation and Purification Technology 250*, 117-209. https://doi.org/10.1016/j.seppur.2020.117209

Ali, A., Macedonio, F., Drioli, E., Aljilil, S. and Alharbi, O.A. (2013). Experimental and theoretical evaluation of temperature polarization phenomenon in direct contact membrane distillation. *Chemical Engineering Research and Design 91*, 1966-1977. https://doi.org/10.1016/j.cherd.2013.06.030

Alkhudhiri, A., Darwish N. and Hilal, N. (2012). Membrane distillation: A comprehensive review. *Desalination 287*, 2-18. https://doi.org/10.1016/j.desal.2011.08.027

Alves, V.D. and Coelhoso, I.M. (2007). Study of mass and heat transfer in the osmotic evaporation process using hollow fibre membrane contactors. *Journal of Membrane Science 289*, 249-257. https://doi.org/10.1016/j.memsci.2006.12.005

Al-Obaidani, S., Curcio, E., Macedonio, F., Di Profio, G., Al-Hinai, H. and Drioli, E. (2008). Potential of membrane distillation in seawater desalination: thermal efficiency, sensitivity study and cost estimation. *Journal of Membrane Science 323*, 85-98. https://doi.org/10.1016/j.memsci.2008.06.006

Bui, V.A., Nguyen, M.H. and Muller, J. (2005). Characterization of the polarizations in osmotic distillation of glucose solutions in hollow fibre module. *Journal of Food Engineering 68,* 391-402. https://doi.org/10.1016/j.memsci.2008.06.006

Bui, V.A., Vu, L.T.T. and Nguyen, M.H. (2010). Modelling the simultaneous heat and mass transfer of direct contact membrane distillation in hollow fiber modules. *Journal of Membrane Science 353*, 85-93. https://doi.org/10.1016/j.memsci.2010.02.034

García-Chávez, R.J., Chávez-Ramírez, A.U., Villafán-Vidales, H.I., Velázquez-Fernández, J.B. and Hernández-Rosales, I.P. (2020). Thermal study of a solar distiller using computational fluid dynamics (CFD). *Revista Mexicana de Ingeniería Química 19*, 455-467. https://doi.org/10.24275/rmiq/IE671

Gryta, M. (2012a). Effectiveness of water desalination by membrane distillation process. *Membranes 2*, 415-29. https://doi.org/10.3390/membranes2030415

Gryta, M. (2012b). Polyphosphates used for membrane scaling inhibition during water desalination by membrane distillation. *Desalination 285*, 170-176. https://doi.org/10.1016/j.desal.2011.09.051

He, F., Sirkar, K.K. and Gilron, J. (2009). Effects of antiscalants to mitigate membrane scaling by

direct contact membrane distillation. *Journal of Membrane Science 345*, 53-58. https://doi.org/10.1016/j.memsci.2009.08.021

Hou, D., Dai, G., Wang, J., Fan, H., Luan, Z. and Fu, C. (2013). Boron removal and desalination from seawater by PVDF flat-sheet membrane through direct contact membrane distillation. *Desalination 326*, 115-124. https://doi.org/10.1016/j.desal.2013.07.023

Ibrahim, S. and Alsalhy, Q. (2013). Modeling and simulation for direct contact membrane distillation in hollow fibre modules. *AIChE J 59,* 589-603. https://doi.org/10.1002/aic.13845

Kebria, M.R.S. and Rahimpour, A. (2020). Membrane Distillation: Basic, advances and applications. *Advances in membrane Technologies, IntechOpen*. https://doi.org/10.5772/intechopen.86952

Ketrane, R., Saidani, B., Gil, O., Leleyter, L. and Baraud, F. (2009). Efficiency of five scale inhibitors on calcium carbonate precipitation from hard water: Effect of temperature and concentration. *Desalination 249*, 1397-1404. https://doi.org/10.1016/j.desal.2009.06.013

Lee, K.P., Arnot, T.C. and Mattia, D. (2011). A review of reverse osmosis membrane materials for desalination-development to date and future potential. *Journal of Membrane Science 370*, 1-22. https://doi.org/10.1016/j.memsci.2010.12.036

Li, B. and Sirkar, K.K. (2005). Novel membrane and device for vacuum membrane distillation based desalination process. *Journal of Membrane Science 257*, 60-75. https://doi.org/10.1016/j.memsci.2004.08.040

Martinez-Diez, L., Florido-Diaz, F.J. and Vázquez-Gonzalez, M.I. (2000). Study of polarization phenomena in membrane distillation of aqueous salt solutions. *Separation Science and Technology 35,* 1485-1501. https://doi.org/10.1081/SS-100100237

Martínez, L. and Vázquez, M.I. (1999). Temperature and concentration polarization in membrane distillation of aqueous salt solutions. *Journal of Membrane Science 156*, 265-273. https://doi.org/10.1016/S0376-7388(98)00349-4

Martínez, L., Vázquez, M.I. and Florido F.J. (1998). Temperature polarization coefficient in membrane distillation. *Separation Science and Technology 33*, 787-799. https://doi.org/10.1080/01496399808544876

Mengual, J.I., Ortiz de Zarate, J.M., Pena, L. and Velazquez, A. (1993). Osmotic distillation through porous hydrophobic membranes. *Journal of Membrane Science 82*, 129-140. https://doi.org/10.1016/0376-7388(93)85098-H

Naidu, G., Jeong, S., Vigneswaran, S., Hwang, T., Choi, Y. and Kim, S. (2015). A review on fouling of membrane distillation. *Desalination and water treatment 57*, 1-25. https://doi.org/10.1080/19443994.2015.1040271

National Centers for Environmental Information. Gulf of Mexico Data Atlas: Seawater Salinity. Retrieved from: https://www.ncei.noaa.gov/maps/gulf-data-atlas/atlas.htm

Peng Y., Ge J., Li Z. and Wang S. (2015). Effects of anti-scaling and cleaning chemicals on membrane scale in direct contact membrane distillation process for RO brine concentrate. *Separation and purification technology 154*, 22-26. https://doi.org/10.1016/j.seppur.2015.09.007

Peñaranda López, A., Martínez Alvarado, J., Muvdi Nova, C. and Torrestiana Sánchez, B. (2016). Development and validation of a theoretical model for osmotic evaporation. *Desalination 384*, 52-59. https://doi.org/10.1016/j.desal.2016.01.035

Rivas-Perez, R., Sotomayor-Moriano, J., Pérez-Zuñiga, C.G. and Calderón-Mendoza, E.M. (2016). Design of a multivariable GPC base don an industrial PC for control of a reverse osmosis unit of a pharmaceutical industry. *Revista Mexicana de Ingeniería Química 15*, 259-273.

Shirazi, M., Kargari, A. and Tabatabaei, M. (2014). Evaluation of commercial PTFE membranes in desalination by direct contact membrane distillation. *Chemical engineering and processing: Process intensification 76*,

16-25. https://doi.org/10.1016/j.cep.2013.11.010

Song, L., Li, B., Sirkar, K.K. and Gilron, J.L. (2007). Direct contact membrane distillation-based desalination: novel membranes, devices, larger-scale studies and a model. *Industrial & Engineering Chemistry Research 46*, 2307-2323. https://doi.org/10.1021/ie0609968

Valdés, H., Romero, J., Saavedra, A., Plaza, A. and Bubnovich, V. (2009). Concentration of noni juice by means of osmotic distillation. *Journal of membrane Science 330*, 205-213. https://doi.org/10.1016/j.memsci.2008.12.053

Warsinger, D.M., Swaminathan, J., Guillen-Burrieza, E., Arafat, H.A. and Lienhard, J. (2015). Scaling and fouling in membrane distillation for desalination applications: a review. *Desalination 356*, 294-313. https://doi.org/10.1016/j.desal.2014.06.031

Zhang, P., Knötig, P., Gray, S., and Duke, M. (2015). Scale reduction and cleaning techniques during direct contact membrane distillation of seawater reverse osmosis brine. *Desalination 374*, 20-30. https://doi.org/10.1016/j.desal.2015.07.005

Zhu, J., Jiang, L. and Matsuura, T. (2015). New insights into the fabrication of hydrophobic/hydrophilic composite hollow fibers for direct contact membrane distillation. *Chemical Engineering Science 137*, 79-90. https://doi.org/10.1016/j.ces.2015.05.064

Appendix A: Concentration polarization in membrane distillation: Assumptions and equations

In the MD process, the concentration polarization coefficient (ζ) has been defined as (Martínez and Vázquez 1999):

$$\zeta = C_{mF}/C_F$$

where C_{mF} is the salt concentration at the feed-membrane interface and C_F is the salt concentration in the feed bulk solution.

The thin-film theory has been used to describe the mass transfer in the feed boundary layer in membrane distillation (Martínez at al., 2000; Bui *et al*., 2010) and osmotic distillation (Mengual *et al*., 1973; Bui *et al*., 2005). In DCMD only water is removed through the membrane, therefore the solute concentration at the membrane surface (C_{mF}) becomes higher than in the bulk solution. In a hollow fiber configuration, C_{mF} can be determined as (Bui et al,. 2010):

$$C_{mF} = C_F \exp \frac{J(r_i/r_o)}{\rho_F K_F}$$

where K_F is the feed mass transfer coefficient and it can be obtained from the dimensionless Sherwood number:

$$K_F = \frac{Sh_F D_{S-W}}{d_h}$$

where D_{S-W} is the diffusion coefficient of the solute. The Sherwood number Sh_F was estimated using the following expression when the feed flows outside the fibers (Alves & Coelhoso 2007; Peñaranda López *et al*. 2016, Ahmad *et al*., 2020):

$$Sh_F = 15.4 Re_F^{0.92} Sc_F^{0.33} \left(\frac{d_h}{L}\right)$$

where Sc is the Schmidt number defined as $Sc_F = \mu_F/(\rho_F D_{S-W})$.